Origin of tweed texture in the simulation of a cuprate superconductor

1993 J. Phys.: Condens. Matter 5 497

(http://iopscience.iop.org/0953-8984/5/4/018)

J. Phys.: Condens. Matter 5 (1993) 497–518. Printed in the UK

Origin of tweed texture in the simulation of a cuprate superconductor

K Parlinski†‡§¶, Volker Heine‡ and E K H Salje†§

† IRC Superconductivity, Madingley Road, Cambridge CB3 0HE, UK
‡ Cavendish Laboratory, Madingley Road, Cambridge CB3 0HE, UK
§ Department of Earth Sciences, University of Cambridge, Downing Street, Cambridge CB2 3EQ, UK
¶ Institute of Nuclear Physics, ulica-Radzikowskiego 152, 31-342 Cracow, Poland

Received 22 April 1992, in final form 10 September 1992

Abstract. The origin of metastable tweed texture (microstructure) is studied by computer simulation. A two-dimensional model of 99 × 99 unit cells represents a layer with an oxygen deficit of the high-T_c superconductor $YBa_2Cu_3O_{7-\delta}$ and exhibits the ferroelastic tetragonal–orthorhombic phase transition. The tweed texture is known to be important for flux pinning. In the model, the local ordering of the oxygen atoms produces long-range strain fields, which have been studied computationally by a molecular dynamics technique. The system has a strong tendency to form the tweed texture, as observed experimentally. Well above the structural phase transition temperature, the strain fluctuations show well developed embryos of the tweed texture, whose temperature dependence agrees with theoretical estimates obtained using the independent-site approximation. On quenching to below the transition temperature, the texture first becomes more regular in spacing *and coarsens before the system orders macroscopically: the kinetics behaviour is quite* different from the traditional model of nucleation and growth.

1. The role of local strain coupling

The purpose of this paper is to study via a computational two-dimensional (2D) model the origin of metastable tweed texture or microstructure attending the structural phase transition (from tetragonal to orthorhombic) in $YBa_2Cu_3O_{7-\delta}$ (YBCO). Part of the motivation for our study is that the tweed texture appears to increase the critical current of superconducting YBCO, presumably by helping to pin flux lines (see, for example, Iqbal *et al* 1989). But tweed texture is a much wider phenomenon, occuring in such diverse materials as feldspars (Wruck *et al* 1991) and metallic alloys (e.g. Fujita 1990), and we believe our study illuminates its origin more generally. The occurrence of tweed depends on the macroscopic strain involved in the phase transition, tetragonal–orthorhombic in the case of YBCO (Marais *et al* 1991a, b, Salje and Parlinski 1991, Salje 1991, Semenovskaya and Khachaturyan 1991), and we have previously shown that the kinetics of phase transitions involving substantial strain is quite different from the traditional nucleation and growth model. The latter work was done on a 3D computer sample of size 15 × 15 × 15 unit cells, hardly large enough to catch the tweed texture (Marais *et al* 1991a, 1992a, b), so that the present 2D sample of 99 × 99 unit cells with a sixfold larger lateral dimension provides a significant rounding-out of the picture. All of these considerations contributed to our choice of

0953-8984/93/040497+22$07.50

YBCO for study since its particular layer structure makes a 2D model appropriate, as will be discussed below.

By strain coupling in a structural phase transition we mean in the present context that the local ordering in one unit cell results in a stress tending to deform that cell and its neighbours, due to the sizes or dispositions of the ordering atoms or groups of atoms such as NO_3^- ions (Reeder *et al* 1988, Salje *et al* 1985, Salje 1990). In the case of YBCO the deformation is an $x^2 - y^2$ type of strain of the tetragonal high temperature unit cell. The tweed texture consists of long thin domains of 'plus' and 'minus' ordering running along (1,1,0) and (1,−1,0) planes so that they criss-cross at right angles. More generally tweed only arises (Marais *et al* 1991a) when that deformation has the symmetry of a macroscopic strain and indeed locally is that strain. The conditions for the occurrence of tweed and other types of texture, including no texture, have been discussed elsewhere (Marais *et al* 1992a, b). It is known that the strain energy can be a substantial fraction of the total energy involved in such a structural phase transition (Salje 1990). The local strain due to ordering in one cell propagates through the elastic deformation of the material to distant cells (Marais *et al* 1991a). One consequence is that the strain fluctuations average the degree of order in a region of cells so that they display a smoother structure than the fluctuations of the occupation itself, as we shall see from our simulation order parameter ρ and a strain order parameter η. For short-range fluctuations η is smoother than ρ, but for long-wavelength fluctuations they are proportional. Another consequence of strain propagating through the medium is that the local ordering in one cell is 'felt' in distant cells, leading to different kinetics of the phase transition as already mentioned (Salje 1990, 1991).

At about 770 K the $YBa_2Cu_3O_{7-\delta}$ crystal undergoes a ferroelastic structural phase transition from tetragonal $P4/mmm$ to orthorhombic $Pmmm$ symmetry. We will use T_c to relate to this transition, not the superconducting one. The T_c depends on the degree δ of oxidation, and on substitutional impurities (Jorgensen *et al* 1987a, b, Alford *et al* 1989). The structural phase transition is nearly second order, with a large spontaneous strain leading to a pronounced (1,1,0) type of microtwinning, at a length scale of some 100 Å (Roth *et al* 1987). The detailed form of the microstructure and its scale depend on the thermal history, on the value of δ and on the concentration of substitutional impurities. Basically it consists of stripe domains (i.e. $(1,\pm1,0)$ platelets in three dimensions, seen as stripes in electron microscopy with the beam parallel to the c axis) or patches of tweed texture. For example, cobalt acts as a local perturbation which favours the orthorhombic deformation and results in a very fine irregular tweed.

The YBCO crystal is usually considered as a quasi-2D structure, consisting of sandwiches of three layers stacked along the c axis. Only one of them has a composition $CuO_{1-\delta}$ which is deficient in oxygen, with $(1-\delta)$ oxygen atoms occupying two oxygen sites per copper atom. In the following we shall confine ourselves to such layers. Since δ is small, we shall ignore it in our model and consider the oxygen sites in this layer to be half-occupied. At the present stage we are interested in the basic origin of the tweed and associated phenomena, not with its variation with detailed composition. The copper atoms form a square lattice and the two oxygen sites lie half-way between the copper atoms along the x and y axes (see figure 1). At high temperatures above T_c the oxygen diffuses over all the sites, giving an average tetragonal symmetry but locally a randomly distorted lattice. The latter is evidenced by the Debye–Waller ellipsoids for the oxygen in x-ray diffraction, which are several

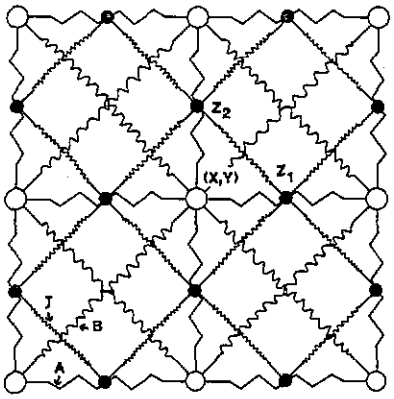

Figure 1. The two-dimensional model used in the computer simulation. The unit cell contains one copper atom (open circles) connected by spring force constants A, B and two oxygen sites (full circles) with interaction J.

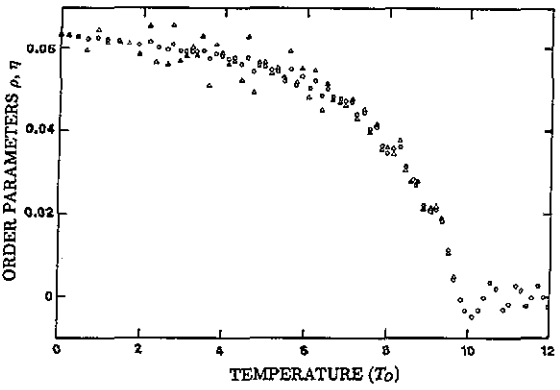

Figure 2. The temperature behaviour of the global strain (triangles) and occupation (circles) order parameters. The transition temperature is $T_c = 9.65T_0$.

times larger than those for oxygen in the other stoichiometric layers (Schmahl *et al* 1988).

At lower temperatures the oxygen in our deficit layer tends to occupy only the sites on the x axis or those on the y axis, and in this way forms one of the two possible domains of the orthorhombic phase with the lattice constant along the occupied axis becoming longer. The order parameter for the transition measures the difference in the occupation probability of the x and y sites. Its symmetry is given by the irreducible representation B_{1g} at $k = 0$ of the space group $P4/mmm$. It has the same symmetry as the e_{xx}–e_{yy} component of the strain tensor so that the two order parameters are coupled, leading to a ferroelastic phase transition. Microscopically it is intuitively obvious that the presence (absence) of an oxygen atom between two copper atoms will lengthen (shorten) the Cu–Cu distance. Symmetry requires that only two types of ferroelastic orthorhombic domain can arise, elongated along the x or y axis respectively, consistent with our microscopic picture above.

The continuity condition for the crystal lattice tells us that macroscopic coherent boundaries between different domains can only exist along the two diagonal planes (1,±1,0). Sapriel (1975) has studied the general conditions for the existence of coherent domain boundaries between domains of different shear, and the above result follows from the general theory when applied to domains of positive and negative shear of type $x^2 - y^2$. Even these boundaries entail some strain energy (Marais *et al* 1992b). The direction of coherent domain boundaries can easily be deduced in two dimensions. Let n_i (in the suffix notation) be a unit vector along the boundary, and $\eta_{ij}(1)$, $\eta_{ij}(2)$ the spontaneous strains on two sides. At any point Rn_i on the boundary, the displacement u_i is $\eta_{ij}\, Rn_j$ and the component of this parallel to the boundary has to be the same for the boundary to remain coherent:

$$\eta^{(1)}_{ij} Rn_j n_i = \eta^{(2)}_{ij} Rn_j n_i \tag{1.1}$$

that is

$$(\eta^{(1)} - \eta^{(2)})_{ij} n_i n_j = 0. \tag{1.2}$$

In our case we have $\eta^{(2)} = -\eta^{(1)}$ with $\eta^{(1)}$ being an elongation (contraction) along the $X(Y)$ direction and $\eta^{(2)}$ the opposite:

$$\eta_{ij}^{(1)} = \begin{bmatrix} \alpha & 0 \\ 0 & -\beta \end{bmatrix} \qquad \eta_{ij}^{(2)} = \begin{bmatrix} -\beta & 0 \\ 0 & \alpha \end{bmatrix}. \tag{1.3}$$

Substitution of (1.3) into (1.2) easily yields for n_i the (1,±1) directions. In 3D the condition (1.2) still holds but n_i is now any vector in the boundary plane (Sapriel 1975).

In order to guide the reader through the details that folow, we will outline here the main ideas and results.

After setting up the computer model in section 2, we compute some straightforward results with it in section 3, which are both of interest in their own right and serve to test the model against some of the experimental results on YBCO. How does the order parameter vary with temperature below T_c? Our model has two ingredients, as does the real YBCO. If one oxygen site in a unit cell is occupied by an oxygen atom, then the other site is unlikely to be occupied also. We represent this by an 'antiferro' coupling J between nearest-neighbour sites. But we have discussed elsewhere (Marais *et al* 1991a, 1992a, b; future publications are planned by these authors) that the local strain set up around an occupied site propagates through elastic relaxation to distant sites, resulting in a long-range coupling between sites. These two mechanisms give a different temperature dependence, and we compare the computer model and experiment with them. Another result relates to the disorder among the oxygen sites, namely the observed anomalously large 'thermal' ellipsoid for the oxygen atoms in the analysis of the structure from x-ray diffraction.

In section 4 we present our evidence from the model for the origin of the tweed texture. There are well defined embryos of the tweed at temperatures well above T_c. We show results at $1.75T_c$ but have seen the same kind of embryos for all runs at temperatures above T_c. In fact it requires a quantitative analysis to see the variation with T above T_c: to visual inspection the colour plates (e) to (h) in Salje and Parlinski (1991) and Salje (1991) look much the same, representing temperatures from $1.1T_c$ to $1.59T_c$. It is quite clear from various tests that these embryos are equilibrium fluctuations of the order parameter and not due to any thermal history or non-equilibrium conditions in our computer runs. Why are they so prominent at temperatures where a nearest-neighbour Ising model would be almost completely disordered? It is necessary to distinguish here between the conventional local order parameter $\rho(r)$ relating to the occupation probability of the oxygen site at r, and the strain order parameter $\eta(r)$ formed from the degree of strain of the individual crystal cells. The $\rho(r)$ is indeed highly disordered, or so it appears at first sight. But $\eta(r)$, because of the long-range nature of strain, effectively integrates $\rho(r)$ over a region of cells and shows that there is a net ordering over a mesoscopic range. Conversely we can argue that such mesoscopic ordering fluctuations at such high temperatures are the result of a cooperation between many unit cells linked by the long-range interaction mediated by strain. A full analysis awaits some development of theory and more detailed simulation results, both currently being pursued (Bratkovsky 1992a). In section 5 we present the traditional theory of the width of the correlation function $S(q)$ at $T > T_c$, and show that our simulation results agree satisfactorily with it.

In section 6 we turn to the ordering kinetics when a sample is quenched from above to below T_c. There are two main aspects, one being the development of

the mesoscopic tweed texture. We will show one figure to indicate the variety of phenomena, namely with the texture first becoming more regular, then coarsening and finally giving way to macroscopic uniform ordering. The details of these processes will be taken up in a separate publication (Parlinski *et al* 1992b), culminating in a so-called time–temperature–transition (TTT) plot.

What section 6 is mainly concerned with is a broader issue. In previous work (Marais *et al* 1991a, 1992a, b) it was shown that the long-range nature of the strain coupling between sites leads to a radically different ordering kinetics from the conventional 'nucleation and growth' behaviour of a nearest-Ising model (and no doubt some real materials). New kinetic rate equations are required (Salje 1988, 1991, Marais *et al* 1991b). Our previous discussion was based on computer simulations with a small model of $15 \times 15 \times 15$ unit cells, which was observed to order homogeneously all over with no delay for nucleation. Clearly that picture now has to be elaborated to take into account the mesoscopic texture.

Finally in section 7 we draw together our concluding remarks.

2. The computational model

The two-dimensional structure for our computer model consists of a square lattice of copper atoms at lattice sites (i,j). There are two oxygen sites per (i,j) unit cell, one lying half-way between copper atoms (i,j) and $(i+1,j)$ on the X axis, to be referred to as site 1 or the X site, and site 2 (or the Y-site) half-way between copper atoms (i,j) and $(i,j+1)$ on the Y axis (figure 1). The potential energy of the model is

$$V = V_{\text{elastic}} + V_{\text{intersite}} + V_{\text{occupation}} \tag{2.1}$$

$$V_{\text{elastic}} = \sum_{i,j} \Big[A(R_{i,j;i+1j} - a_0 - \alpha Z_{i,j}^{(1)})^2 + A(R_{i,j;i,j+1} - a_0 - \alpha Z_{i,j}^{(2)})^2 + B(R_{i,j;i+1,j+1} - a_0\sqrt{2})^2 + B(R_{i,j;i+1,j-1} - a_0\sqrt{2})^2 \Big] \tag{2.2}$$

$$V_{\text{intersite}} = \sum_{i,j} J \left(Z_{i,j}^{(1)} Z_{i+1,j}^{(2)} + Z_{i,j}^{(1)} Z_{i+1,j-1}^{(2)} + Z_{i,j}^{(2)} Z_{i,j}^{(1)} + Z_{i,j}^{(2)} Z_{i,j+1}^{(1)} \right) \tag{2.3}$$

$$V_{\text{occupation}} = \sum_{i,j} \left\{ -E \left[(Z_{i,j}^{(1)})^2 + (Z_{i,j}^{(2)})^2 \right] + G \left[(Z_{i,j}^{(1)})^4 + (Z_{i,j}^{(2)})^4 \right] \right\} \tag{2.4}$$

$$R_{ij;i'j'} = [(X_{i,j} - X_{i'j'})^2 + (Y_{i,j} - Y_{i'j'})^2]^{1/2} \tag{2.5}$$

where a_0 is the lattice constant and (X_{ij}, Y_{ij}) the position vector of copper atom (ij). In (2.2) each copper atom is coupled to its nearest and next-nearest copper atoms by harmonic springs with spring constants A and B respectively. This choice of forces guarantees that the phonon normal modes form two acoustic branches and hence that the structure behaves correctly as an elastic medium, as is essential for modelling the strain effects mentioned in section 1.

The treatment of the oxygen atoms is a little unusual. Consider the double-well function

$$f(Z) = -EZ^2 + GZ^4 \tag{2.6}$$

with minima at

$$Z_0 = \pm(E/2G)^{1/2} \tag{2.7}$$

where Z is for the moment some abstract non-spatial variable describing some system. If the double well is very deep relative to the thermal energy k_BT, then the variable Z is always very near one of the two values $\pm Z_0$, i.e. it behaves practically like an Ising variable $\sigma = \pm 1$ apart from the scaling factor Z_0. As usual, we can use an Ising variable to denote the occupancy of a site by an oxygen atom, $\sigma = +1$ for site occupied and $\sigma = -1$ for site empty. Similarly we can use the variable Z in (2.6) as an oxygen site occupation variable: we call it a 'soft Ising' variable, with $Z_{ij}^{(1)}$ and $Z_{ij}^{(2)}$ referring to sites 1 and 2 in cell (ij). The practical advantage of this device is that the Zs are continuous variables which can be treated by molecular dynamics in the simulation, on the same footing as the X_{ij}, Y_{ij}. Otherwise one would have to treat the system in a mixed way, Monte-Carlo sampling for the discrete σ variables and molecular dynamics for the X_{ij}, Y_{ij}, which is possible (Marais *et al* 1991a) but more cumbersome and time consuming. To be sure, for computational efficiency one must not really have the double well (2.6) very deep, and one must postulate some fictional associated kinetic energy $\frac{1}{2}M(\mathrm{d}Z/\mathrm{d}t)^2$, but this does not change the qualitative behaviour of the system. To summarize, the term (2.4) in the potential represents the occupancy of the oxygen sites. It has incidentally another function: it introduces anharmonicity into the model and hence ensures thermal equilibrium in the phonon system during a simulation run.

The interaction between oxygen atoms occurs in two ways. Firstly when one site is occupied, its nearest-neighbour sites are likely to be unoccupied because of Coulomb repulsion. Remember that only about half the oxygen sites are occupied (section 1). This effect is described by (2.3) with positive (repulsive) J, directly analogous to an antiferromagnetic nearest-neighbour Ising model. Secondly the $\alpha Z_{i,j}^{(1)}$, $\alpha Z_{i,j}^{(2)}$ in the first two terms of (2.2) give a lengthening by αZ_0 of a nearest-neighbour Cu–Cu distance when the intervening site is occupied, and a shortening by $-\alpha Z_0$ when unoccupied. Such local strain is of course propagated through the lattice by the V_{elastic}, and through the same effect acts as a force on distant $Z_{i',j'}^{(1)}$, $Z_{i',j'}^{(2)}$. We can make this more explicit by expanding the first term of (2.2) to give

$$A(R_{i,j;i+1,j} - a_0)^2 - 2A\alpha Z_{i,j}^{(1)} \text{ (times displacements of atoms at } i,j \text{ and } i+1,j) + \text{(higher-order terms)} \tag{2.8}$$

and similarly the second term of (2.2). Expansion (2.8) now has the same form as in the model considered by Marais *et al* (1991a, 1992a, b). The bilinear term in αZ gives a force on the copper atoms for a given $Z_{i,j}^{(1)}$, and conversely a force on the occupation variable $Z_{i,j}^{(1)}$ for a given displacement of the copper atoms.

The 2D spatial symmetry of the potential (2.1) is $P4mmm$, as is the system ensemble symmetry for equal random occupation of the oxygen sites. When the X sites are occupied more than the Y sites, the system elongates in the X direction and shortens along Y, i.e. it develops a positive shear of $X^2 - Y^2$ type and has symmetry $Pmm2$. Similarly preferential occupation of the Y sites gives a negative shear of the same type. Some more complex spin models coupled to the lattice, in similar fashion to ours, lead to first-order transitions (Takahashi 1988a, b). However,

ours maps directly onto the simple so-called phi-four model (Padlewski *et al* 1992) as will be discussed below. It therefore gives a continuous transition.

The numerical values of the potential parameters $A = 2000$, $B = 8000$, $J = 2500$, $E = 3000$, $\alpha = 1.0$ and $G = 10^6$ have been chosen so that the ground-state configuration of the model has a required symmetry $Pmm2$ and the lattice deformation is about 6%. The anharmonic force constant G fixes the magnitude of the displacement amplitude. Introducing the lattice constants $R_{i,j;i+1,j} = X_0$, $R_{i,j;i,j+1} = Y_0$, $R_{i,j;i+1,j+1} = (X_0^2+Y_0^2)^{1/2}$, $Z_{i,j}^{(1)} = Z_0^{(1)}$ and $Z_{i,j}^{(2)} = Z_0^{(2)}$, one finds the numerical values of the ground-state rectangular unit cell to be $X_0 = 1.0626a_0$, $Y_0 = 0.9356a_0$, $Z_0^{(1)} = 0.0632a_0$ and $Z_0^{(2)} = -0.0633a_0$.

We return to the issue of using soft Ising variables Z_μ rather than discrete Ising spins, where we use the suffix μ as an abbreviation for indices i, j and 1 or 2. There are several points to be made. At the time of this work (1990) some tests were successfully carried out which showed that the results are very similar to a much more time-consuming code using discrete spins (Marais 1990). Subsequent work with an improved code for discrete spins gives tweed patterns which appear to the eye indistinguishable from those described here (Bratkovsky 1992b). The quantitative effects of coupling in the z direction to give a three-dimensional model are also being studied. Soft Ising models such as the present one (or the phi-four model as it is often called) can display either soft-mode or order–disorder behaviour at the phase transition depending on the values of the parameters. The position of the crossover has been determined by Padlewski *et al* (1992), and we can show that the present parameters place our model somewhat on the order–disorder side by mapping it onto the phi-four model by a two-step argument. First we expand the first two terms of (2.2). The resulting terms in Z_μ^2 can be grouped with those in (2.3) to give the total on-site quadratic potential

$$\sum(\alpha A^2 - E)Z_\mu^2. \tag{2.9}$$

The terms from (2.2) which are linear in Z_μ can be treated in the manner of Marais *et al* (1991a) to decouple the lattice completely and give an effective interaction $J_{\mu\nu}Z_\mu Z_\nu$ between occupation variables. With the above values for the parameters, the coefficient in (2.9) is negative, which places the model in the order–disorder regime (Padlewski *et al* 1992) and this qualitatively like a discrete Ising spin.

The model has been simulated using the molecular dynamics technique (Parlinski 1987, 1988, 1989). The crystallite consisted of 99×99 unit cells with 29 205 particles. Free boundary conditions were used, with edges of the crystallite cut along (1,0) directions and consisting of copper only. The free boundary conditions allow the domain walls to flow in and out of the crystallite. The Newton equations of motion were solved iteratively by a simple difference scheme with time step $\Delta t = 0.002\tau_0$. The canonical ensemble with constant temperature (Dove 1988) has been used. The temperature has been defined by an average kinetic energy. There, at each iteration step the particle velocities were corrected by a factor $(T_d/T)^{1/2}$, where T_d is the desired temperature of the system and T is the currently calculated temperature.

We have set the units of length to the lattice constants $a_0 = 1$, the particle mass $M_0 = 1$ and time unit $\tau_0 = 1$. Hence, the energy and temperature units are $T_0 = M_0 a_0^2 \tau_0^{-2}$, and the parameters A, B, H, E and G are in $M_0\tau_0^{-2}$ and $M_0\tau_0^{-2}a_0^{-2}$ units, respectively.

3. Straightforward results and test of the model

We now discuss some results of the model which are of some interest in their own right in relation to YBCO and at the same time provide some test of the model.

First there is the variation of the order parameter with temperature T below T_c, and the determination of T_c itself. We define local values of the order parameters ρ_{ij}, η_{ij} which are a measure of the oxygen site occupation and the strain respectively at lattice site (i,j):

$$\rho_{ij} = \tfrac{1}{4}(\langle R_{i,j;i+1,j}\rangle + \langle R_{i,j;i-1,j}\rangle - \langle R_{i,j;i,j+1}\rangle - \langle R_{i,j;i,j-1}\rangle) \tag{3.1}$$

$$\eta_{i,j} = \tfrac{1}{4}\left(\langle Z^{(1)}_{i,j}\rangle + \langle Z^{(1)}_{i-1,j}\rangle - \langle Z^{(2)}_{i,j}\rangle - \langle Z^{(2)}_{i,j-1}\rangle\right). \tag{3.2}$$

Note that in (3.1) we want the difference between the occupancy of the X and Y sites because the phase transition is a condensation of the oxygen atoms on the X or the Y sites. In (3.1), (3.2) the $\langle \ldots \rangle$ denotes a short time average over an interval of order $\Delta t = 0.05\tau_0$, i.e. over 25 time steps. The corresponding global order parameters are

$$\langle \rho \rangle = \frac{1}{N}\sum_{i,j}\langle \rho_{i,j}\rangle \tag{3.3}$$

$$\langle \eta \rangle = \frac{1}{N}\sum_{i,j}\langle \eta_{i,j}\rangle. \tag{3.4}$$

Here N is the total number of cells taken in the summation from which we have excluded one edge row of cells all round to minimize edge effects.

Figure 2 gives the temperature variations of the global $\langle \rho \rangle$ and $\langle \eta \rangle$ on one cooling and one heating run. Both runs were sufficiently slow with $|dT/dt| = 0.075(T_0/\tau_0)$ that at each temperature the system was sufficiently close to equilibrium. The heating run was started from a single domain equilibrated at temperature 2.5 T_0, so that points below 2.5 T_0 in figure 2 are from the cooling run only.

We first note from figure 2 that the values of the order parameters at $T = 0$ are in good agreement with the values $\rho(T=0) = 0.0633$ and $\eta(T=0) = 0.0634$ calculated from the ground-state lattice constants X_0, Y_0 and occupation variables $Z^{(1)}_0$, $Z^{(2)}_0$ obtained by minimizing the potential energy (2.1). The fact that the two order parameters are normalized to the same value at $T = 0$ stems from the use of the coefficient $\alpha = 1.0$ in (2.2). Secondly the values of $\rho(T)$ and $\eta(T)$ are strictly proportional over all T, in fact equal with our normalization. Thirdly we note that the transition temperature $T_c \simeq 9.65T_0$ both on heating and cooling. This value falls between two simplified approximate theoretical estimates of 15.0 T_0 and 5.0 T_0 made in section 5. Fourthly the non-zero values of the order parameter in figure 2 above T_c represent fluctuations from the finite sample size. The values for the occupation order parameter are about three times larger than $\rho(T=0)N^{-1/2}$ because of the coherent embryo regions (section 4). Fifthly the curve just below T_c may be depressed because the transition around the corners of the sample occurs already at a temperature lower than T_c. To limit the effect of sample size, the outer row of cells has been omitted as mentioned below (3.4) but may extend further into the sample, especially at corners.

It is of some interest to make a theoretical interpretation of the variation of the order parameter below T_c. We start with the simulations and compare with

experiment subsequently. Our computer model is a mixed model. If we set $\alpha = 0$ in (2.2) we cut out the strain coupling, leaving only the nearest-neighbour interaction J (2.3) between sites. On the other hand, setting $J = 0$ in (2.3) leaves only a long-ranged coupling between sites, mediated by strain and the motion of the copper atoms (Marais *et al* 1991a, 1992a, b). Another feature is that we have replaced the discrete Ising occupation variable by the 'soft Ising' well (2.6), (2.4). Our first comparison in figure 3 is therefore with the 2D Ising model for which the order parameter $Q(T)$ is given by (Huang 1987)

$$Q(T) = \left\{1 - \sinh^{-4}[(T_c/T)\,\mathrm{arcsinh}\,1]\right\}^{1/8}. \tag{3.5}$$

This curve lies far too high in the diagram, with a rather sharp variation just near T_c. We therefore turn to the opposite extreme, still an Ising model but now treated in the Bragg–Williams approximation (mean field theory) which is known to become exact in the limit of a long-ranged coupling:

$$Q\,(T) = \tanh[(T_c/T)Q]. \tag{3.6}$$

This is seen to be much closer to the simulation data (figure 3), which is not surprising in view of what we shall see later, namely that the strain effect controls the equilibrium fluctuations and the ordering kinetics. As remarked above, the strain effect leads to an effective long-range interaction which is what is needed for the validity of (3.6). We now turn to the fact that the simulations have a 'soft Ising' variable (2.4), (2.6), whereas both (3.5) and (3.6) apply to an Ising spin. The 'soft' case has been treated by Salje *et al* (1991), still assuming long-ranged coupling (i.e. mean field theory). The solution of the model requires a further approximation and the result is also shown in figure 3 (normalized to unity at $T = 0$) with the parameters of Salje *et al* (1991), $\Delta = 1$ and $\eta = 0$. Their quantum parameter η is set equal to zero because there are no quantum effects in the simulations. This curve is seen to fit the best. However, it fits by no means perfectly, which we ascribe to the approximation in the solution of Salje *et al* (1991), to the fact that our model does not map exactly on theirs, to disordering near the corners just below T_c, and that the interaction in the simulation has both long-ranged and nearest-neighbour parts. Moreover the long-ranged strain effects are very anisotropic.

We conclude from the foregoing discussion that the rather 'slow' or 'soft' variation of the order parameter between $T = 0$ and T_c in the model is largely the result of the long-ranged interactions between oxygen sites, due to the local strain set up by the oxygen ordering. The variation of the order parameter in figure 3 lies well below the curve of the nearest-neighbour 2D Ising model with its rapid change just below T_c, and we would expect that to apply to the real system. However, the occupancy of the oxygen sites in the real material would be described by a proper Ising variable rather than the 'soft' Ising coordinate (2.6) of our model. That would raise the curve in figure 3 a little for the order parameter in the real material, as follows from the work of Salje *et al* (1991). We therefore expect the real material to follow approximately the Bragg–Williams curve in figure 3.

We turn now to a comparison of the model with experiment. There is a major difficulty here: the oxygen content of the material tends to vary with temperature, and T_c is quite sensitive to oxygen content. Corrections to the data would require detailed knowledge of the exact conditions of the heating process, the oxygen fugacity

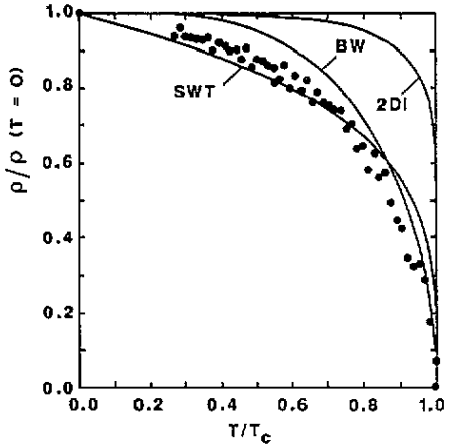

Figure 3. The variation with temperature of the site occupancy order parameter in reduced units. Points, simulation model; full curves, theoretical models; BW, Bragg–Williams; 2DI, two-dimensional Ising model; SWT, model of Salje, Wruck and Thomas (1991) with parameters $\Delta = 1$ and $\eta = 0$.

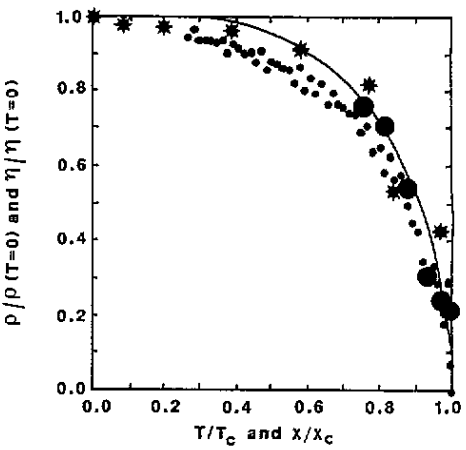

Figure 4. The variation of the order parameters in reduced units. Points, simulation model; full circles, temperature variation of strain in quenched samples from Jorgensen *et al* (1987a, b); stars, variation of strain with substituted cobalt concentration x (after Schmahl *et al* 1989); full curve, Bragg–Williams approximation.

of the sample cell, etc. Such information is not available for published experimental data (e.g. Jorgensen *et al* 1987a, b). We have therefore chosen some other strain measurements by Jorgensen *et al* (1987a, b), namely those on rapidly quenched samples, which hopefully minimizes the chemical variations. These results are shown in figure 4. They lie a little above the simulation results, close to the Bragg–Williams curve, as expected for the reasons discussed above.

We make one other comparison with experiment in figure 4 of a rather different nature. The substitution of a small concentration x of Co for Cu lowers T_c dramatically so that the spontaneous strain (degree of tetragonality) is zero at room temperature for $x > x_c = 0.025$. Thus the normalized order parameter as a function of x/x_c in the alloys at room temperature mimics the variation with T/T_c in the pure material. The data of Schmahl *et al* (1989) are included in figure 4 plotted that way. Because all the alloy specimens were heat treated together and measured at room temperature, the disturbance due to variation of oxygen content should be minimal. These results also fit the Bragg–Williams curve fairly well (figure 4). The substitution of x/x_c for T/T_c is not rigorous in general, of course. However, it is easy to show that it is correct if we have some order parameter $Q(T, x)$ obeying the simplest Landau law

$$Q^2(T, x) = a[T - T_c(x)]/2B \tag{3.7}$$

where a and B are constants and $T_c(x)$ varies linearly

$$T_c(x) = T_{c0} - \alpha x. \tag{3.8}$$

The normalized $Q^2(T, x)$ is then always a straight line as a function of T/T_c or x/x_c. The agreement in figure 4 therefore adds general confidence to our earlier

conclusion. This is not insignificant because temperature data uncorrected for change of oxygen content follow a very different curve which we believe must be discounted.

The second type of relevant experimental data is the disordered displacement of the copper atom in the tetragonal phase, as seen in the thermal ellipsoid in the x-ray structure analysis (Schmahl *et al* 1988). Part of this is due to the normal thermal vibration of the atom and part due to the push or pull from the adjacent oxygen sites depending on whether they are occupied or empty. The mean square displacement in the X direction is given by U_{11}. For the copper atom in the layers of composition CuO_2 this has the value $U_{11} = 0.0045$ Å^2 which we take to be due to atomic vibrations only. Actually this is an overestimate of the vibrational displacement because according to the x-ray analysis there are some oxygen vacancies also in that layer. The U_{11} for copper in our layer with composition $CuO_{0.30}$ is 0.0206 Å^2, from which we subtract the vibrational part estimated above to give $U_{11}(\mathrm{st})$ from structural disorder of 0.015 Å^2.

Now consider a copper atom and its two adjacent oxygen sites in the X direction. The copper atom will remain undisplaced if both sites are occupied or both empty, but there will be a displacement which we take to be of order $\pm\alpha Z_0$ when one site is occupied and the other not. The probability of the latter is $2p(1-p)$ where $p = 0.30$ is the occupation probability of a site in the specimen of Schmahl *et al* (1988). Our estimate of $U_{11}(\mathrm{st})$ is therefore

$$U_{11}(\mathrm{st}) = 2p(1-p)(\alpha Z_0)^2. \tag{3.9}$$

We obtain two different values depending on what we take for Z_0^2. If we use (2.7) we have $U_{11}(\mathrm{st}) = 0.009$ Å^2; on the other hand the use of $Z_0^{(1)} = 0.0633a_0$ from the actual shear of the structure at $T = 0$ gives $U_{11}(\mathrm{st}) = 0.025$ Å^2. These two values straddle the experimental value which we regard as sufficient to establish the effect. We expect $U_{11}(\mathrm{st})$ for the in-between oxygen atom to have a similar magnitude to that of the copper atom, as observed. However, the very large U_{22} for this oxygen refers to motion perpendicular to the Cu–Cu direction: it is due presumably to Coulomb repulsion from other nearby O^{2-} ions, and is so large because there is no other atom in that direction for it to 'bump into'.

4. Fluctuations of the order parameter and the origin of tweed texture

We have already shown elsewhere that our computer model gives beautiful tweed texture when one quenches a computer sample from above T_c to below it (Salje and Parlinski 1991, Salje 1991). The purpose of this section and section 6 is to throw further light on the origin of the texture in terms of recognizable 'embryos' of the tweed texture occurring as equilibrium fluctuations of the order parameter at temperatures at least as high as $1.75T_c$. This is well above T_c and as high as we looked.

In order to show the fluctuations, it is convenient to draw colour maps of the order parameter distributions of $\rho_{i,j}$ and $\eta_{i,j}$. As discussed in section 3, each of these order parameters varies between ± 0.0633, which are more or less extreme values although locally slightly larger values occur occasionally. We therefore take the range between -0.07 and $+0.07$, and divide it into 16 equal intervals, to which we assign colour gradations from red to dark green, respectively. The data sets $\{\rho_{i,j}\}$ and $\{\eta_{i,j}\}$

defined in (3.1), (3.2) at some typical instant of time (but averaged over the small interval $0.05\tau_0$) were placed on a regular grid of 99×99 unit cells and contour lines drawn of constant order parameter values corresponding to the 16 intervals defined above. The grid was not corrected for the lattice shear below T_c. The areas between the contour lines were then filled by the appropriate colours. Hence red and green regions correspond to the two oppositely sheared domains with the yellow lines being the domain walls.

We first show the comparison between the occupation $\rho_{i,j}$ and strain $\eta_{i,j}$ order parameters at $T = 1.38T_c$ in figure 5, where figure 5(*a*) gives the strain and figure 5(*b*) the occupation variable. Comparing the two maps, one notices that red and green regions tend to correspond to each other, which shows that broadly speaking the occupation and strain order parameters are coupled to one another. Individual red and green regions, always enclosed by yellow lines, are limited to a few lattice constants in extent. The strain fluctuations are very anisotropic in shape, sometimes even of needle form, with domain walls predominantly oriented along the [1,±1] directions (diagonals of the figures). The fluctuations of the occupation order parameter are more isotropic, with more short-wavelength variation; however, even here the domain boundaries tend to lie in the [1,±1] directions, but with more 'roughening' of the boundaries.

Taken together with figure 2, the above discussion may be summarized by saying that the occupation and strain order parameters are proportional to one another for long-wavelength fluctuations, in fact equal in our normalization (section 3). At short wavelength the strain order parameter is smoother, so that in future figures we shall only use it as showing the character of the fluctuations with less 'noise'. As already indicated in section 1, this is qualitatively easy to understand: the strain from any one site propagates proportional to $(R_{i,j})^{-3}$ through the elastic medium consisting (in the model) of copper atoms, so that the local strain at one cell is the sum of influences from the occupation of sites over a small region. A quantitative theory is under development (Bratkovsky 1992*c*).

Figure 6 shows how the fluctuations extend to high temperatures well above T_c. Figure 6(*a*) pictures the strain order parameter at $1.06T_c$. As one would expect so close to T_c, there are large amplitude fluctuations: note the occurrence of the extreme red and green colours. Figure 6(*b*) shows the fluctuations at a much higher temperature $1.75T_c$. As expected, there is more disorder but there are still fluctuations with the maximum amplitude. This is surprising. Whereas locally an Ising occupation variable only has the values ±1 and our 'soft' Ising variable some value near $\pm Z_0$, the strain integrates over several lattice sites as we have emphasized and need not locally be anywhere near its maximum or minimum values. In fact we might have expected the map of strain fluctuations at such a high temperature to show only small amplitude variations.

We conclude from figure 6 that at high temperatures above T_c, as high as one is likely to anneal at and quench from, the strain fluctuations show well developed embryos of tweed texture. As well as being tweed-like in shape, the local strain in them often attains the maximum value equal to that of the fully ordered material at low temperature. The same can be seen at intermediate temperatures $1.10T_c$ to $1.59T_c$ in Salje and Parlinski (1991). In fact these figures are almost indistinguishable from some of the metastable tweed texture resulting after quenching in the same model. There is no doubt that the embryos existing above T_c before quenching become the metastable tweed texture after quenching, with a small or

large development in form, of course, depending on the other conditions, i.e. rate of quench, final temperature and time held there.

Figure 7 shows an interesting sequence of strain maps in a single (green) domain of the rectangular phase below T_c. They are taken from a simulation run starting effectively at zero temperature and heated slowly. Care was taken to equilibrate the system at the recorded temperatures. The sequence shows that the nature of the equilibrium disorder below T_c again has the same kind of structure of needle-like micro-domains running along the $[1,\pm1]$ directions. Of course close to T_c (figure 7(*d*)) the amplitude of the strain fluctuations becomes large enough that they sometimes reach the value characteristic of an oppositely ordered (red) domain. Since this was a heating run, the observed texture cannot possibly result from nucleation at higher temperature.

We conclude from this section that disorder in our model, at all temperatures above and below T_c and over the whole sample, is dominated by strain-induced micro-domains with boundaries approximately parallel to $[1,\pm1]$. The embryos above T_c, which become the tweed texture after quenching, are not some special regions having some special type of disorder. On the contrary, there is practically no other type. We suggest, as one consequence, that the metastable tweed texture below T_c probably has a free energy not very much higher than the equilibrium one. We also note that a typical length of a micro-domain fluctuation in figure 6 is of order $20a_0 \approx 75$ Å, comparable to what is seen in the finest tweed texture (Schmahl *et al* 1989).

5. Quantitative treatment of fluctuations

The purpose of this section is to develop some very simplified theory of the fluctuations above T_c, and to analyse some of the simulation results in terms of it. With slightly different approximations it will also give two estimates of the transition temperature T_c.

In our system the ordering of the N oxygen atoms on the $2N$ oxygen sites is the primary ordering process, so we shall focus on it. Fluctuations are commonly discussed in terms of the Landau free energy which, to a sufficient approximation above T_c, has the form

$$G(T,Z) = G_0 + \frac{1}{2}\sum_{k} \Omega(k,T)Z(k)Z(-k). \tag{5.1}$$

Here we use the Fourier components $Z(k)$ of the occupation variables $Z_{i,j}^{(l)}$ with $l = 1, 2$ on the two sites per unit cell at positions $r_1 = (a_0/2, 0)$, and $r_2 = (0, a_0/2)$ relative to the copper atom, defined by

$$\langle Z_{i,j}^{(l)} \rangle = (-1)^l \sum_{k} Z(k) \exp \mathrm{i}[2\pi k(R_{i,j}^0 + r_l)]. \tag{5.2}$$

The Landau free energy (5.1) is derived with the aid of the Bogolyubov inequality

$$G \leqslant G_0 + (V - V_0)_0 \tag{5.3}$$

where G_0 is the calculable free energy of some simple system and $V - V_0$ the rest of the potential energy. The $\langle \ldots \rangle_0$ denotes an expectation with respect to the distribution corresponding to G_0. We can employ this for a Landau free energy functional because it is simply a free energy with the expectation value of the order parameter constrained to have some preset value $Z(k)$.

We now use the independent-site approximation (Bruce 1980), i.e. choose V_0 to be $V_{\text{occupation}}$ (2.4). The corresponding G_0 is

$$G_0 = 2Ng_0^0(T) + \frac{1}{2}\sum_{ijl} \chi_0^{-1}(Z_{i,j}^l)^2 = 2Ng_0^0(T) + N\sum_k \chi_0^{-1} Z(k)Z(-k) \tag{5.4}$$

where g_0^0 is the free energy of a single particle in the well (2.6) in the absence of any external force. Here χ_0 is the susceptibility of such a particle to an external force and is given by the universal relation (Bruce 1980)

$$\chi_0(T) = \langle Z^2 \rangle^{(0)}/k_B T \tag{5.5}$$

where $\langle \ldots \rangle^{(0)}$ is the fluctuation at temperature T in the absence of an external force. The role of V_{elastic} (2.2) in the ordering process is to give a long-range effective interaction between site occupancies (Marais *et al* 1991a), which is difficult to treat theoretically. We therefore ignore it and for our approximation take $V - V_0$ in (5.3) as $V_{\text{intersite}}$ (2.3), so that the Landau free energy becomes

$$G = 2Ng_0^0(T) + N\sum_k \Omega(k,T)Z(k)Z(-k) \tag{5.6a}$$

where

$$\Omega(k,T) = k_B T/\langle Z^2 \rangle^{(0)} + J(k) \tag{5.6b}$$

and

$$J(k) = -2J[\cos \pi(k_x + k_y)a_0 + \cos \pi(k_x - k_y)a_0]. \tag{5.6c}$$

We can now make an estimate of T_c, defined as usual by the condition

$$\Omega(k = 0, T_c) = 0. \tag{5.7}$$

We have $k = 0$ in (5.7) corresponding to the minimum of $J(k)$, the fact that one site in each cell is occupied while the other is empty being taken care of by the factor $(-1)^l$ in (5.2). From (5.7) we have

$$k_B T_c = 4J\langle Z^2 \rangle^{(0)}. \tag{5.8}$$

For the well (2.6) we have, especially for a deep well representing an Ising variable,

$$\langle Z^2 \rangle^{(0)} \approx Z_0^2 = E/2G = 0.0015 \tag{5.9}$$

which gives $T_c = 15.0T_0$, rather higher than the value $9.65T_0$ obtained from the simulation. This difference is due, at least partly, to our approximation of ignoring

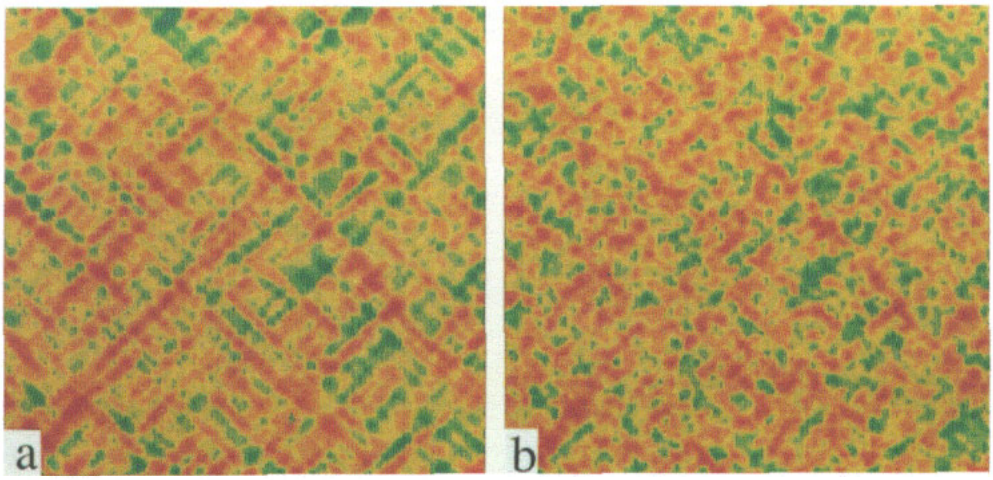

Figure 5. The maps of (*a*) strain and (*b*) occupation order parameter fluctuations taken at $T = 1.38T_c$. Note that strain fluctuations are elongated along the (1,1) directions (main diagonals of the maps) while spin fluctuations are more isotropic.

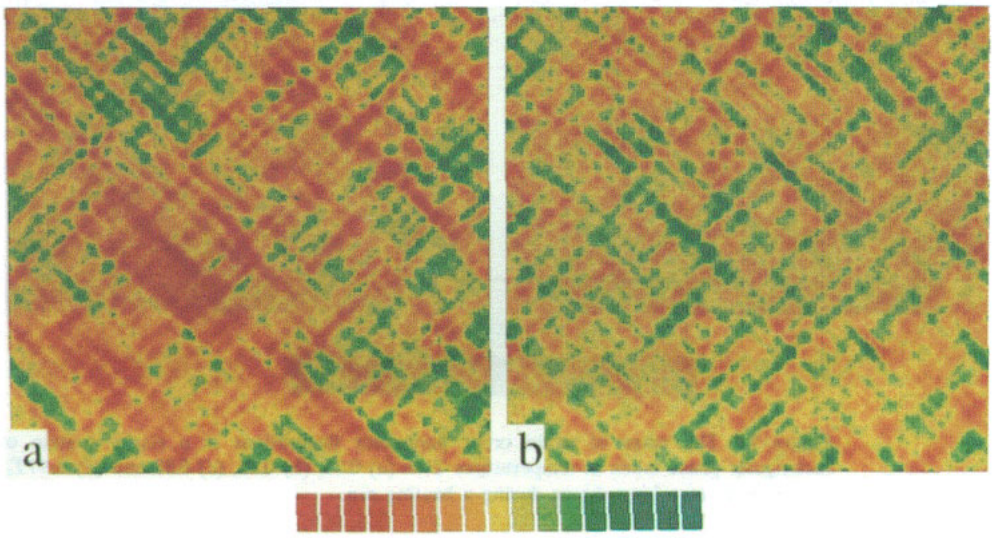

Figure 6. A comparison of the maps of strain order parameter fluctuations at two temperatures (*a*) $T = 1.06T_c$ and (*b*) $T = 1.75T_c$. The large dynamic fluctuations may serve as embryos of domains in a quenching process.

the strain subsystem (2.2). Indeed if one assumes all copper atoms to be fixed at the lattice sites, i.e. $R_{i,j;i+1,j} = a_0$ etc, then the total potential at each oxygen site becomes $(A - E)Z^2 + GZ^4$, giving

$$\langle Z^2 \rangle^{(0)} = (E - A)/2G = 0.0005. \tag{5.10}$$

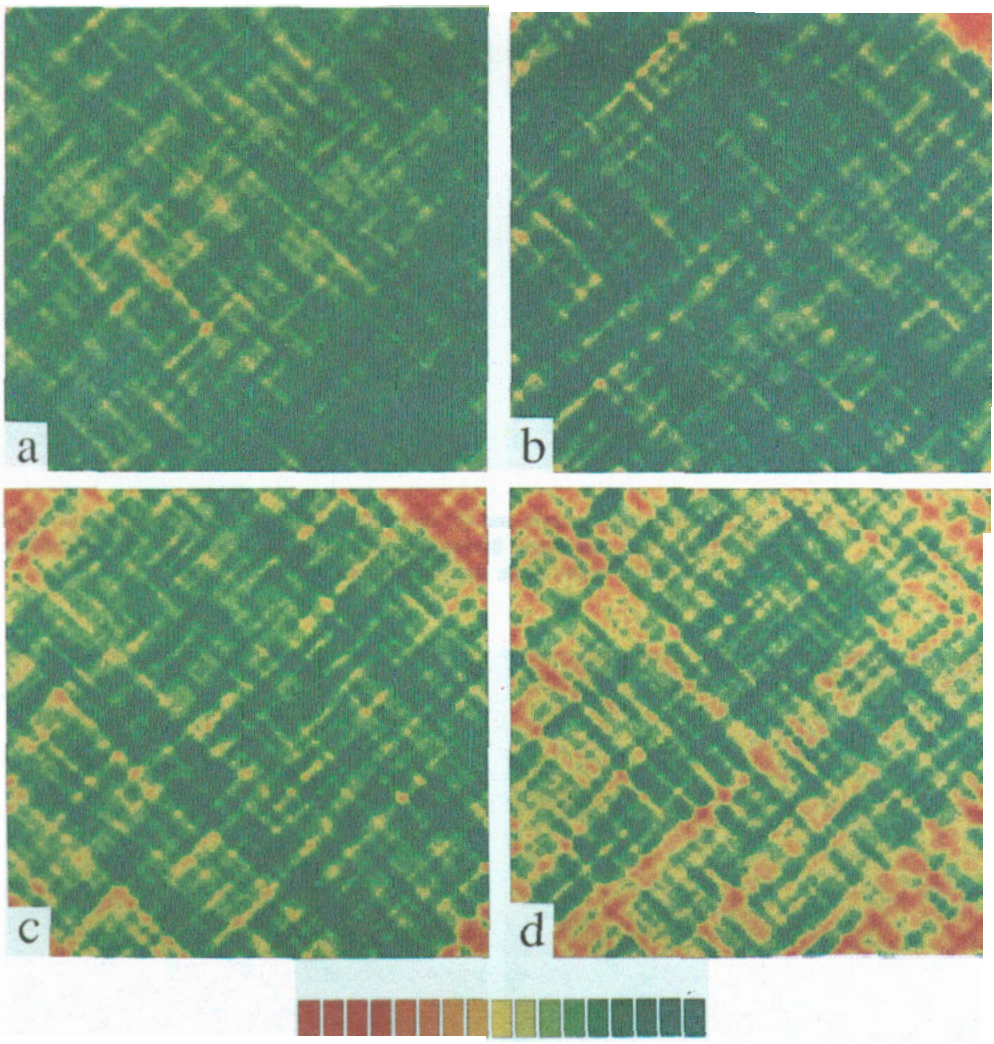

Figure 7. The maps of strain order parameter fluctuations in a single domain of rectangular phase taken at temperatures T = (*a*) 0.75, (*b*) 0.83, (*c*) 0.88 and (*d*) $0.97T_c$. These maps have been drawn during a heating run.

This gives $T_c = 5.0T_0$, a value now too low. We can be satisfied that the two estimates from (5.9) and (5.10) bracket the correct value.

We can now apply (5.6) to the characteristics scale Γ_q^{-1} of the fluctuations. In view of the fluctuation boundaries running perpendicular to the $(1,\pm1)$ directions, we confine our analysis to k in these directions, $k = (q/\sqrt{2}, \pm q/\sqrt{2})$. For these k we have

$$\Omega(k,T) = (\langle Z^2\rangle^{-1})k_B(T - T_c) + 8\pi^2 J q^2. \tag{5.11}$$

The amplitude of the fluctuations is obtained by giving $\frac{1}{2}k_BT$ of free energy to each degree of freedom in (5.6*a*):

$$\tfrac{1}{2}k_B T = \left[(\langle Z^2\rangle^{(0)})^{-1}k_B(T - T_c) + 8\pi^2 J q^2\right]\langle Z(q)Z(-q)\rangle \qquad (5.12)$$

$$S(q) \equiv \langle Z(q)Z(-q)\rangle = (\text{const})\Gamma_q/(q^2 + \Gamma_q^2) \qquad (5.13)$$

with

$$\Gamma_q = (1/2\pi)[k_B(T - T_c)/2J\langle Z^2\rangle^{(0)}]^{1/2} = 0.058\sqrt{T - T_c} \qquad (5.14)$$

where we have used (5.9). In (5.13) $S(q)$ is the occupation correlation function of Lorentzian form, corresponding to exponential decay in real space with decay length Γ_q^{-1}. Note that the proportionality constant in (5.13) influences only the amplitude and not the width of the Lorentzian.

We can now apply the fluctuation theory (5.13), (5.14) to the results of the simulations. A Fourier analysis of the fluctuations has been made at several temperatures and a Lorentzian fitted as shown in figure 8. The Lorentzian form is seen to describe the fluctuations quite well. Then figure 9 compares $\Gamma_q(T)$ with the result (5.14), which is seen to fit moderately well, particularly as regards the magnitude, which contains no adjustable parameter. The length of a typical fluctuation will be of order $2\Gamma_q^{-1}$ (one decay length from the centre in each direction) which is of order $20a_0$ at higher temperatures, and this indeed accords visually with figure 6(*b*). We have already noted that $20a_0 \approx 75$ Å is of the right order of magnitude to describe the experimentally observed tweed texture at its finest (Schmahl *et al* 1989, Putnis *et al* 1987, Wruck *et al* 1991).

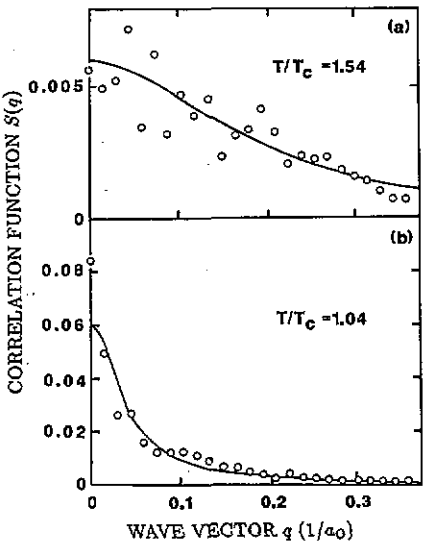

Figure 8. The correlation function $S(q)$ of the occupation order parameter as a function of the wave vector q in the [1,1] direction at two temperatures.

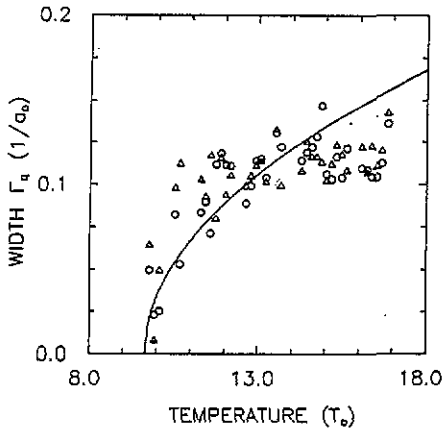

Figure 9. The width Γ_q of the Lorentzian fitted to the correlation function $S(q)$ of the occupation order parameter in the square phase above T_c. The circles and triangles correspond to the [1,1] and [−1,1] directions, respectively. The full curve shows the theoretical curve (equation (5.14)).

Actually our analysis is somewhat fraudulent. An expansion of (5.6c) around $k = 0$ yields (5.11) for any direction of k where $q = |k|$. That would lead to

large circular fluctuation patches of diameter $2\Gamma_q^{-1}$ with correspondingly smaller amplitude. We have of course ignored the strain subsystem (2.2) and that would inhibit fluctuations for k not along $(1,\pm1)$ very severely. We speculate that we have obtained the right order of magnitude for the length of the micro-domains because the strain effect does not hinder the extent of a fluctuation there. What is less clear is what controls the widths of the micro-domains. It is evident that the strain effect is singular around $k = 0$ and a much more sophisticated theory will be required.

6. Ordering kinetics with strain coupling

As outlined in section 1, we here consider two questions, firstly the development of the tweed texture from the fluctuation embryos, and secondly the issue of phase transformation kinetics more generally in the presence of strain effects.

The development of tweed texture depends on many factors, particularly time and the quench temperature. A fuller treatment will be given elsewhere (Parlinski *et al* 1992b) based on our simulation model, culminating in a TTT diagram (time, temperature and transformation), including comparison with experiment. Here we only give an indication of the qualitative phenomena seen, to round up the role of the embryos seen at high temperature, which have been the main focus of this paper.

Figure 10 shows the development in time of $S(q)$ as defined above (equation (5.11)). Already at $t = 0$ after a very rapid quench from 1.35 T_c to 0.62 T_c, the $S(q)$ has changed from a Lorentzian centred on $q = 0$ to a peak at $qa_0 \simeq 0.8$. In real space this corresponds to the texture becoming more regular. The spacing between the domain walls becomes even more regular as the peak of $S(q)$ sharpens further at $t = 0.1\tau_0$ (figure 10). The tweed pattern taking up a rather regular spacing presumably minimizes (locally) the strain energy in the same sense as a regular crystal structure can be said to minimize interatomic strain energy. The $S(q)$ is very small at q well beyond the peak and near $q = 0$, meaning that each domain is uniformly ordered. Finally the peak moves towards $q = 0$ as one domain orientation wins over the other.

We turn now to the second issue. In earlier simulations with a very similar model (Marais *et al* 1991a, 1992a, b), it was noted that the kinetics of the phase transformation became very different from the traditional nucleation-and-growth model when the intercell interaction was largely mediated by strain effects: in fact the kinetics became very much faster and more uniform. What can we say about this picture in the light of the present work? The earlier conclusions were based on a cubical model of $15 \times 15 \times 15$ cells, whereas the present one of 99×99 cells has a much wider spatial extent on account of being two-dimensional, although the number of cells has only been about doubled. We recall that the earlier interpretation was that each cell 'feels' the ordering in every other cell due to the long range (infinite range) of the strain-mediated interaction. Thus the sample ordered uniformly without forming nuclei or domains.

Clearly we need to re-examine this story in the light of the present work. Domains *are* formed, and they are nucleated by the embryos existing at all temperatures. Two points need to be made to update the earlier picture. First of all, as already indicated, the interior of each domain rapidly achieves a uniform degree of order and we interpret this as being caused by the strain coupling as before. Secondly the growth of tweed texture around embryos and subsequent overall ordering of the sample in

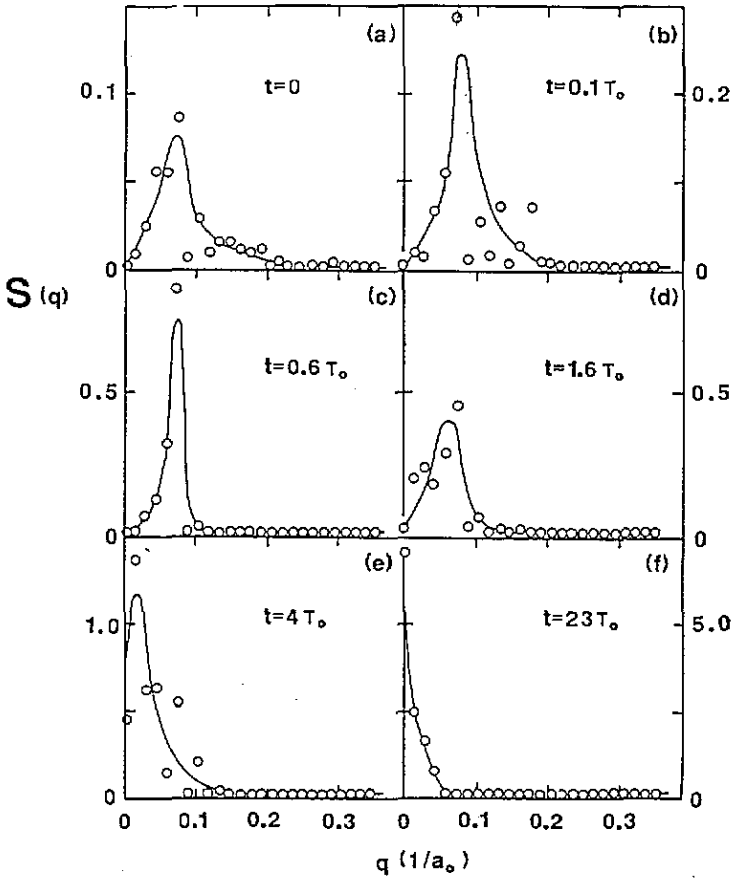

Figure 10. The evolution with time of the correlation function $S(q)$ in the [1.1] direction at an annealing temperature of $0.62T_c$, after a quench from $1.35T_c$.

the present work are very different from the *traditional* nucleation and growth model. The crux of the latter was that it took a long time for fluctuations to create a nucleus larger than the critical size needed for it to grow, the critical size being a result of the mismatch in some sense between the ordered interior of the nucleus and the disordered exterior. Imagine what happens to the classical picture if the nuclei are always automatically larger than the critical size. In this case there is no activation barrier or time lag to their growth, as found in this work. We may summarize by saying that in our simulation model there are always fluctuations or embryos of tweed texture everywhere which serve as nuclei for growth of order, but they are of such a nature that there is no barrier to their growth on quenching the sample. In all this the strain coupling plays a crucial role. In particular, the interior of one domain over a length scale of order 10 lattice spacings orders uniformly and rapidly, as found previously.

7. Concluding remarks

We have found that a remarkably simple model has immediately given a rich

microstructure of tweed texture without the need for fine tuning, including the coarsening of the tweed, replacement by stripe domains and final annealing into one domain. Some of these details will be elaborated elsewhere (Parlinski *et al* 1992b), the main point here being the origin of the tweed. The model consists only of a lattice of copper atoms connected by springs to make an elastic medium, with oxygen sites between the copper atoms. It was not necessary to complicate the model by making the oxygen atoms part of the elastic medium; their only role is that when an oxygen site is occupied by an oxygen atom it pushes the adjacent copper atoms apart, whereas when the site is empty the copper atoms are pulled together somewhat. The ordering of the available oxygen atoms on the sites (we consider the case of half as many atoms as sites) therefore leads to a local strain in the elastic medium, and corresponding macroscopic strain in one domain of the ordered phase below the transition temperature T_c. That local strain and its elastic propagation through the medium govern all the phenomena. Positive and negative values for the order parameter lead to positive and negative shear of symmetry $x^2 - y^2$. The main factor is that domain boundaries cost a large amount of strain energy unless they lie perpendicular to the (1,±1,0) directions. Actually our model is only two dimensional, to represent a layer of YBCO, but the same geometrical requirement applies in two and three dimensions and indeed the simulation results are similar (Bratkovsky 1992d). Our model is therefore an extension of an earlier one by Wen *et al* (1981) who produced tweed-like patterns by forming rectangular unit cells with two orientations into a 2D layer, and permitting them to undergo a reconfiguration so as to decrease the elastic energy. The difference is that in our case the orientations of the unit cells are controlled by proper statistical mechanics of the oxygen atoms.

Our most significant result is that strong equilibrium fluctuations exist above T_c at temperatures as high as we have investigated, up to $1.75T_c$. Their form can best be described as embryos of the tweed texture, namely a criss-cross of needle-like domains lying in the (1,±1) directions in our 2D model. The strain inside each domain is comparable with the macroscopic strain of the ordered structure at $T = 0$. There are not just a few such embryos here and there: on the contrary, they are ever-present throughout the material at all temperatures. Indeed simulations of the equilibrium state below T_c have shown that the partial disorder there also has a similar form. The requirements of the local strain mean that no other type of disorder in practice exists. Above T_c such a type of disorder has been observed as the streaking of Bragg peaks in x-ray scattering measurements (Jiang *et al* 1991). Around such embryos the tweed texture grows if one quenches the computer sample from above to below T_c.

A single needle domain in the fluctuations above T_c has a length typically of 20 lattice constants, i.e. of order 75 Å, and a width $2.5a_0$ to $3a_0$ of order 10 Å. The tweed texture on quenching starts in this sort of scale. For example, Jiang *et al* (1991) have found from diffuse x-ray scattering that in $YBa_2(Cu_{0.955}Al_{0.045})_3O_7$ crystals the correlation range of the oxygen ordering, i.e. the size of the structure which locally remains orthorhombic, is ~ 40 Å; Putnis *et al* (1987) find ⩾ 25 Å, and Zhu *et al* (1990) report 30–50 Å. This factor may be important in high-temperature superconductivity where the superconductivity coherence length in this material is only ~ 15 Å (Xu and Suenaga 1991).

In this paper we have only considered the stoichiometric material $YBa_2Cu_3O_{7-\delta}$ with $\delta = 0$, but it would be trivial to extend the computer model to $\delta > 0$. One would follow paths well trodden in the theory of alloy phase diagrams and no qualitative change in behaviour is expected until δ reaches near unity. Actually it is not the total

oxygen content that is relevant but the δ in the composition $CuO_{1-\delta}$ of the layer responsible for the shear strain, which can differ from that of the overall composition (Schmahl *et al* 1988).

Acknowledgments

The authors wish to thank A Giddy for much help in handling the computer systems, and B Wruck for the graphs of the order parameter in various theoretical models. Fruitful comments on the computer programs by M Dove and B Farid are gratefully acknowledged. One of us (KP) would like to thank the staff of the Department of Earth Sciences, Cambridge, for their hospitality and assistance during a stay there, and to acknowledge the Guest Research Fellowship from the Royal Society and support from SERC through the Cavendish Laboratory and IRC Superconductivity.

References

Alford N McN, Button T W, Gough C E, Wellhofer F, O'Connor D A, Colclough M S, Pollard R J and McCartney D G 1989 *J. Appl. Phys.* **66** 5960

Bratkovsky A 1992a private communication

—— 1992b unpublished

—— 1992c private communication

—— 1992d private communication

Bruce A P 1980 *Adv. Phys.* **29** 111

Dove M 1988 *Physical Properties and Thermodynamic Behaviour of Minerals* ed E K H Salje (Dordrecht: Reidel)(published in cooperation with NATO Scientific Affairs Division) pp 501–90

Fujita F E 1990 *Mater. Sci. Eng.* A **127** 243–8

Huang K 1987 *Statistical Mechanics* (New York: Wiley)

Iqbal Z, Thadhani N, Johnson K A, Rao K V, Ramakrishna B L, Sharma R, Reidinger F and Eckhard H 1989 *Physica* C **162–4** 885

Jiang X, Wochner P, Moss S C and Zschack P 1991 *Phys. Rev. Lett.* **67** 2167

Jorgensen J D, Beno M A, Hinks D G, Soderholm L, Volin K J, Hitterman R L, Grace J D, Schuller I K, Segre C U, Zhang K and Kleefish M S 1987a *Phys. Rev.* B **36** 3608

Jorgensen J D, Veal B W, Kwok W K, Crabtree G W, Umezawa A, Nowicki L J and Paulikas A P 1987b *Phys. Rev.* B **36** 5731

Marais S 1990 private communication

Marais S, Bratkovsky A, Heine V and Salje E K H 1992a *J. Phys.: Condens. Matter* submitted

Marais S, Heine V, Nex C M M and Salje E K H 1991a *Phys. Rev. Lett.* **66** 2480–3

Marais S, Padlewski S and Salje E K H 1991b *J. Phys.: Condens. Matter* **3** 6571–7

Marais S, Salje E K H, Heine V and Bratkovsky A 1992b *J. Mater. Res.* submitted

Mukami *et al* 1989

Padlewski S, Evans A K, Ayling C and Heine V 1992 *J. Phys.: Condens. Matter* **4** 4895

Parlinski K 1987 *Phys. Rev.* B **35** 8690

—— 1988 *Comp. Phys. Rep.* B **8** 153

—— 1989 *Phys. Rev.* B **39** 12 154

Parlinski K, Salje E K H and Heine V 1992a *Acta Metall.* submitted for publication

—— 1992b *Acta Metall.* submitted for publication

Putnis A, Salje E K H, Redfern S A T, Fyfe C A and Strobl H 1987 *Phys. Chem. Miner.* **14** 446–54

Reeder R J, Redfern S A T and Salje E K H 1988 *Phys. Chem. Miner.* **15** 605–11

Roth G, Ewert D, Heger G, Hervieu M, Michel C, Raveau B, D'Yvoire F and Revcolevschi A 1987 *Z. Phys.* **69** 21

Salje E K H 1988 *Phys. Chem. Miner.* **15** 336–48

—— 1990 *Phase Transitions in Ferroelastic and Co-elastic Crystals* (Cambridge: Cambridge University Press) p 336

—— 1991 *Acta Crystallogr.* A **47** 453–69
Salje E K H, Kuscholke B, Wruck B and Kroll H 1985 *Phys. Chem. Miner.* **12** 99–107
Salje E K H and Parlinski K 1991 *Supercond. Sci. Technol.* **4** 93–7
Salje E K H, Wruck B and Thomas H 1991 *Z. Phys.* B **82** 399–404
Sapriel J 1975 *Phys. Rev.* B **12** 5128
Schmahl W W, Putnis A, Salje E K H, Freeman P, Graeme-Barber A, Jones R, Singh K K, Blunt J, Edwards P P, Loram J and Mirza K 1989 *Phil. Mag. Lett.* **60** 241–8
Schmahl W W, Salje E K H and Liang W Y 1988 *Phil. Mag. Lett.* **58** 173
Semenovskaya S and Khachaturyan A G 1991 *Phys. Rev. Lett.* **67** 2223
Takahashi K 1988a *Z. Phys.* B **71** 205
—— 1988b *Prog. Theor. Phys.* **77** 997
Wen S, Morris J W and Khachaturyan A G 1981 *Metall. Trans.* A **12** 581
Wruck B, Salje E K H and Graeme-Barber A 1991 *Phys. Chem. Miner.* **17** 700–10
Xu Y and Suenaga M 1991 *Phys. Rev.* B **43** 5516
Zhu Y, Suenaga M and Moodenbaugh A R 1990 *Phil. Mag. Lett.* **62** 51